J Sci Comput
DOI 10.1007/s10915-015-0111-7

Babich's Expansion and High-Order Eulerian Asymptotics for Point-Source Helmholtz Equations

Jianliang Qian[1] · Lijun Yuan[2] · Yuan Liu[1] · Songting Luo[3] · Robert Burridge[4]

Received: 5 December 2014 / Revised: 5 August 2015 / Accepted: 16 September 2015

Abstract The usual geometrical-optics expansion of the solution for the Helmholtz equation of a point source in an inhomogeneous medium yields two equations: an eikonal equation for the traveltime function, and a transport equation for the amplitude function. However, two difficulties arise immediately: one is how to initialize the amplitude at the point source as the wavefield is singular there; the other is that in even-dimension spaces the usual geometrical-optics expansion does not yield a uniform asymptotic approximation close to the source. Babich (USSR Comput Math Math Phys 5(5):247–251, 1965) developed a Hankel-based asymptotic expansion which can overcome these two difficulties with ease. Starting from Babich's expansion, we develop high-order Eulerian asymptotics for Helmholtz equations in inhomogeneous media. Both the eikonal and transport equations are solved by high-order Lax–Friedrichs weighted non-oscillatory (WENO) schemes. We also prove that fifth-order Lax–Friedrichs WENO schemes for eikonal equations are convergent when the eikonal is

✉ Jianliang Qian
qian@math.msu.edu

Lijun Yuan
yuanlijun.ma@gmail.com

Yuan Liu
yliu7@math.msu.edu

Songting Luo
luos@iastate.edu

Robert Burridge
burridge137@gmail.com

1 Department of Mathematics, Michigan State University, East Lansing, MI 48824, USA

2 College of Math and Statistics, Chongqing Technology and Business University, Chongqing 400067, People's Republic of China

3 Department of Mathematics, Iowa State University, Ames, IA 50011, USA

4 Department of Mathematics and Statistics, University of New Mexico, Albuquerque, NM 87131, USA

Published online: 22 September 2015

smooth. Numerical examples demonstrate that new Eulerian high-order asymptotic methods are uniformly accurate in the neighborhood of the source and away from it.

Keywords Eikonal equations · Eulerian asymptotics · Helmholtz equations · High-order factorization

1 Introduction

We consider the Helmholtz equation with variable refractive index $n(\mathbf{r})$. A point-source problem amounts to finding the solution of the equation

$$[\Delta + \omega^2 n^2(\mathbf{r})]w = -\delta(\mathbf{r}, \mathbf{r}_0), \tag{1}$$

where

$$\Delta = \sum_{i=1}^{m} \frac{\partial^2}{\partial x_i^2}, \quad \mathbf{r} = [x_1, x_2, \ldots, x_m]^T, \tag{2}$$

$\mathbf{r}_0$ is the source location, ω is the angular frequency, m is the dimension, and the Sommerfeld radiation condition is imposed at infinity. The point-source solution is the so-called Green's function which is needed for a variety of applications, such as medical imaging, seismic imaging, underwater acoustics, and synthetic aperture radar. When the angular frequency ω is large, it is difficult for finite-difference or finite-element methods to solve the Helmholtz equations accurately because of so-called pollution errors or dispersion errors. Therefore, alternative approaches are sought to compute such solutions. In this paper we develop high-order Eulerian asymptotics for point-source Helmholtz equations in inhomogeneous media by using Babich's expansion [3].

To motivate Babich's formulation, we apply the usual asymptotic expansion of the solution for the Helmholtz equation of a point source in an inhomogeneous medium as

$$w(\mathbf{r}, \mathbf{r}_0) = e^{i\omega\tau} \sum_{s=0}^{\infty} A_s(\mathbf{r}, \mathbf{r}_0) \frac{1}{(i\omega)^{s-\frac{(m-1)}{2}}}, \tag{3}$$

where $\tau = \tau(\mathbf{r}, \mathbf{r}_0)$ is the phase satisfying the eikonal equation

$$\nabla\tau \cdot \nabla\tau = n^2(\mathbf{r}), \quad \tau(\mathbf{r}_0, \mathbf{r}_0) = 0, \tag{4}$$

and $A_s = A_s(\mathbf{r}, \mathbf{r}_0)$ satisfy a recursive system of PDEs,

$$2\nabla\tau \cdot \nabla A_s + A_s \Delta\tau = -\Delta A_{s-1}, \quad s = 0, 1, \ldots, A_{-1} \equiv 0. \tag{5}$$

However, a difficulty arises immediately: how to initialize A_s at the source point for this system of equations. Moreover, when m is even, the ray series (3) does not yield a uniform asymptotic form close to the source. When $m = 3$ Avila and Keller [2] were able to find the initial data for A_s by using the boundary layer method, but the case of $m = 2$ was left incomplete. In practice, such difficulties in initializing amplitudes were handled in ad hoc ways in the sense that the amplitudes were initialized a little bit away from the point source by using amplitudes for the medium with a constant refractive index corresponding to that of the source point [12,15,16,20,24]; consequently, the resulting numerical asymptotic solution is not approximated with uniform accuracy near the source. To overcome these initialization difficulties Babich [3] proposed to use an asymptotic series defined by the first Hankel function as an ansatz to expand the underlying highly-oscillatory wavefield; the

resulting eikonal equation is the same as the usual one, but the resulting transport equations are easily initialized. Moreover, Babich's expansion ensures that the Hankel-based ansatz yields a uniform asymptotic solution as $\omega \to \infty$ in the neighborhood of the point source and away from it.

Based on Babich's expansion, we develop high-order Eulerian asymptotic methods for point-source Helmholtz equations in inhomogeneous media. By Eulerian asymptotics, we mean that we solve the eikonal and transport equations as PDEs and utilize the resulting asymptotic ingredients to construct the asymptotic solution; see [4] for an introduction to Eulerian geometrical optics. To do that we first apply high-order Lax–Friedrichs WENO sweeping schemes to the eikonal equation and transport equations; we further prove that high-order Lax–Friedrichs WENO sweeping schemes for eikonal equations are convergent when the eikonal solution is smooth. Numerical examples demonstrate that the proposed high-order Eulerian asymptotic methods yield uniform asymptotic solutions as ω varies in the neighborhood of the point source and away from it.

2 Babich's Hankel Based Ansatz

To solve Eq. (1) asymptotically when $\omega \to \infty$, Babich [3] proposed the following Hankel-based ansatz to expand the solution u

$$w(\mathbf{r}, \mathbf{r}_0) = \sum_{s=0}^{\infty} v_s(\mathbf{r}, \mathbf{r}_0) f_{s-(m-2)/2}(\omega, \tau), \tag{6}$$

where

$$f_q(\omega, \tau) = i \frac{\sqrt{\pi}}{2} e^{iq\pi} \left(\frac{2\tau}{\omega}\right)^q \mathrm{H}_q^{(1)}(\omega\tau), \tag{7}$$

and τ is the phase satisfying the eikonal equation (4). Here $\mathrm{H}_q^{(1)}$ is the q-th Hankel function of the first kind. The amplitude coefficients v_{s+1} in expression (6) satisfy the recurrent system

$$4\tau n^2 \frac{\partial v_{s+1}}{\partial \tau} + v_{s+1}\left[\Delta\tau^2 + 2n^2(2s + 2 - m)\right] = \Delta v_s, \quad s = -1, 0, 1, \ldots, \tag{8}$$

and $v_{-1} \equiv 0$, where the differentiation $\frac{\partial}{\partial \tau}$ is performed along the ray departing from $\mathbf{r}_0$. Assuming $v_s(\mathbf{r}, \mathbf{r}_0)$ to be continuous in the neighborhood of $\mathbf{r} = \mathbf{r}_0$, we get the initial conditions for v_0 at $\mathbf{r} = \mathbf{r}_0$,

$$v_0(\mathbf{r}, \mathbf{r}_0)|_{\mathbf{r}=\mathbf{r}_0} = \frac{n_0^{m-2}}{2\pi^{(m-1)/2}}, \quad n_0 = n(\mathbf{r}_0). \tag{9}$$

When $n(\mathbf{r})$ is smooth, τ is smooth in the neighborhood of $\mathbf{r}_0$ except the source point itself as shown in [2,17,23]. When $n(\mathbf{r})$ is analytic, it can be shown [3] that the function $v_0(\mathbf{r}, \mathbf{r}_0)$ will also be analytic in $\mathbf{r}$ when $\mathbf{r}$ is in the neighborhood of $\mathbf{r}_0$; furthermore, $v_{s+1}(\mathbf{r}, \mathbf{r}_0)$ are determined in terms of v_0 and τ so that v_{s+1} are analytic when v_0 are analytic for $s = 0, 1, \ldots$. In the following we assume that $\mathbf{r}_0$ is at the origin so that $\mathbf{r}_0$ will be suppressed in the notations.

According to the ray theory or the method of characteristics, we have

$$n^2 \frac{\partial}{\partial \tau} = \nabla\tau \cdot \nabla, \tag{10}$$

$$\Delta\tau^2 = 2\tau\Delta\tau + 2n^2. \tag{11}$$

Using (10) and (11) in (8), we get

$$2\tau\nabla\tau\cdot\nabla v_{s+1}+v_{s+1}[\tau\Delta\tau+n^2(2s+3-m)]=\frac{\Delta v_s}{2},\quad s=-1,0,1,\ldots, \tag{12}$$

or

$$\nabla\tau^2\cdot\nabla v_{s+1}+v_{s+1}\left[\frac{\Delta\tau^2}{2}+n^2(2s+2-m)\right]=\frac{\Delta v_s}{2},\quad s=-1,0,1,\ldots. \tag{13}$$

Although Eqs. (12) and (13) are mathematically equivalent, Eq. (13) is more suitable for computing v_s numerically since τ^2 is smooth at the source point while τ behaves like a distance function and thus is not smooth at the source point. Therefore, Eq. (13) equipped with the initial condition (9) will be numerically solved to yield v_s.

2.1 Relation to the Usual Geometrical-Optics Ansatz

When $s=-1$, Eq. (12) yields

$$2\tau\nabla\tau\cdot\nabla v_0+v_0[\tau\Delta\tau+n^2(1-m)]=0. \tag{14}$$

Setting $v_0=\tau^{\frac{m-1}{2}}A_0$, we have

$$2\nabla\tau\cdot\nabla A_0+A_0\Delta\tau=0, \tag{15}$$

which is the conventional transport equation for the leading coefficient in the usual geometrical-optics ansatz.

Babich's leading term near the source behaves like

$$w\approx v_0\mathrm{i}\frac{\sqrt{\pi}}{2}\mathrm{e}^{-\pi\mathrm{i}\frac{m-2}{2}}\left(\frac{\omega}{2\tau}\right)^{\frac{m-2}{2}}\mathrm{H}^{(1)}_{-\frac{m-2}{2}}(\omega\tau), \tag{16}$$

where v_0 tends to

$$\frac{n_0^{m-2}}{2\pi^{\frac{m-1}{2}}} \tag{17}$$

as the field point tends to the source, n_0 being the value of n at the source.

Inserting (17) into (16) and using formula 9.1.6 in [1] we see that, asymptotically near the source, the wave field that we are trying to approximate is reduced to

$$w\simeq\frac{n_0^{(m-2)}}{2^{\frac{m+2}{2}}\pi^{\frac{m-2}{2}}}\left(\frac{\omega}{\tau}\right)^{\frac{m-2}{2}}\mathrm{i}\,\mathrm{H}^{(1)}_{\frac{m-2}{2}}(\omega\tau); \tag{18}$$

when $m=2$ this reduces to

$$w\simeq\frac{\mathrm{i}}{4}\mathrm{H}^{(1)}_0(\omega\tau), \tag{19}$$

and when $m=3$, to

$$\begin{aligned} w&\simeq\frac{n_0}{2^{\frac{5}{2}}\pi^{\frac{1}{2}}}\left(\frac{\omega}{\tau}\right)^{\frac{1}{2}}\mathrm{i}\,\mathrm{H}^{(1)}_{\frac{1}{2}}(\omega\tau),\\ &=\frac{n_0}{2^{\frac{5}{2}}\pi^{\frac{1}{2}}}\left(\frac{\omega}{\tau}\right)^{\frac{1}{2}}\mathrm{i}\sqrt{\frac{2}{\pi\omega\tau}}(-\mathrm{i})\,\mathrm{e}^{\mathrm{i}\omega\tau}\\ &=n_0\frac{\mathrm{e}^{\mathrm{i}\omega\tau}}{4\pi\tau} \end{aligned} \tag{20}$$

2.2 Two-Term Expansion for the 2-D Case

When $m = 2$, the transport equation (13) is reduced to

$$\nabla\tau^2 \cdot \nabla v_{s+1} + v_{s+1}\left[\frac{\Delta\tau^2}{2} + 2sn^2\right] = \frac{\Delta v_s}{2}. \tag{21}$$

Letting $s = -1$ in the above equation, we have the equation for coefficient v_0,

$$\nabla\tau^2 \cdot \nabla v_0 + v_0\left[\frac{\Delta\tau^2}{2} - 2n^2\right] = 0, \tag{22}$$

with the initial condition for v_0 as

$$v_0(\mathbf{r})|_{\mathbf{r}=\mathbf{0}} = \frac{1}{2\sqrt{\pi}}. \tag{23}$$

Therefore, we can find v_0 by solving Eq. (22) with the initial condition (23). In the homogeneous case ($n(\mathbf{r}) \equiv n_0$), we have $v_0 \equiv \frac{1}{2\sqrt{\pi}}$.

Letting $s = 0$ in (21), we obtain the equation for the coefficient v_1 as

$$\nabla\tau^2 \cdot \nabla v_1 + v_1\frac{\Delta\tau^2}{2} = \frac{\Delta v_0}{2}, \tag{24}$$

with the initial condition for v_1 to be determined according to v_0 and n.

2.3 Two-Term Expansion for the 3-D Case

When $m = 3$, the transport equation (13) is reduced to

$$\nabla\tau^2 \cdot \nabla v_{s+1} + v_{s+1}\left[\frac{\Delta\tau^2}{2} + n^2(2s-1)\right] = \frac{\Delta v_s}{2}. \tag{25}$$

Letting $s = -1$ in the above equation, we have the equation for the coefficient v_0 as

$$\nabla\tau^2 \cdot \nabla v_0 + v_0\left[\frac{\Delta\tau^2}{2} - 3n^2\right] = 0, \tag{26}$$

with the initial condition of v_0 at $\mathbf{r} = \mathbf{0}$,

$$v_0|_{\mathbf{r}=\mathbf{0}} = \frac{n_0}{2\pi}. \tag{27}$$

Therefore, we can find v_0 by solving Eq. (26) with initial condition (27). For the homogeneous medium $n \equiv n_0$, $v_0 \equiv \frac{n_0}{2\pi}$.

Letting $s = 0$ in (25), we have the equation for the coefficient v_1,

$$\nabla\tau^2 \cdot \nabla v_1 + v_1\left[\frac{\Delta\tau^2}{2} - n^2\right] = \frac{\Delta v_0}{2}, \tag{28}$$

with the initial condition for v_1 to be determined.

3 Approximations of Eikonals and Amplitude Coefficients Near the Source

To solve the transport equation (13), we need to solve the eikonal equation for τ first as τ^2 appears as coefficients in the transport equation. At first, we consider to obtain an accurate one-term Babich's asymptotic expansion which requires that v_0 be of at least first-order accuracy. Since $\Delta\tau^2$ appears as a coefficient in the transport equation (13) ($s = -1$) for v_0, numerically computed $\Delta\tau^2$ should be of at least first-order accuracy so that v_0 is of first-order accuracy; this in turn implies that τ^2 itself should be computed with third-order accuracy. Next, we consider to obtain an accurate two-term Babich's expansion. Since the transport equation (13) ($s = 0$) for v_1 involves both $\Delta\tau^2$ and Δv_0 as coefficients and the accuracy of v_0 also depends on that of $\Delta\tau^2$, these facts imply that first-order accurate v_1 needs first-order accurate Δv_0, which in turn implies that v_0 itself should be of third-order accuracy. To have third-order accurate v_0, the transport equation (13) ($s = -1$) for v_0 should have third-order accurate coefficient $\Delta\tau^2$, which implies that τ^2 should have fifth-order accuracy. Consequently, to obtain the two-term Babich's asymptotic expansion for the point-source solution of the Helmholtz equation, we need to use fifth-order schemes to solve the eikonal equation for τ and related higher order schemes to solve the transport equations for v_0 and v_1.

Since initial conditions for the eikonal and transport equations are only specified at the source point and high-order schemes need accurate initial values within a small neighborhood of the source to start with, we will assume that the refractive index n, the eikonal-squared τ^2, and the coefficients v_s are analytic near the source so that we can extract high-order approximations of eikonals and amplitude coefficients near the source.

3.1 High-Order Factorization of Eikonals

Since $\tau(\mathbf{r})$ behaves like the distance function $|\mathbf{r}|$ near the source, it is non-differentiable at the source point so that the local truncation error analysis will fail for finite-difference methods and all formally high-order schemes will only yield first-order accuracy near the source, and the resulting first-order accuracy will propagate through the computational domain because of the upwinding nature of the underlying schemes. To overcome such difficulties, in [15] we have proposed high-order factorization based high-order sweeping methods for point-source eikonal equations, and we further develop this family of high-order methods here.

According to [15], letting $T(\mathbf{r}) = \tau^2$ and $S(\mathbf{r}) = n^2$, we have following expansion near the source point for analytic T and S:

$$T(\mathbf{r}) = \sum_{k=0}^{\infty} T_k(\mathbf{r}), \quad S(\mathbf{r}) = \sum_{k=0}^{\infty} S_k(\mathbf{r}), \tag{29}$$

where $T_k(\mathbf{r})$ and $S_k(\mathbf{r})$ are homogeneous polynomials of degree k in $\mathbf{r}$. More specifically, we can determine T_k term-by-term by substituting the expansions (29) into the squared eikonal equations,

$$T_0 = 0, \quad T_1 = 0, \quad T_2(\mathbf{r}) = S_0\mathbf{r}^2, \quad T_3(\mathbf{r}) = \frac{1}{2}S_1(\mathbf{r})\mathbf{r}^2,$$

$$T_4(\mathbf{r}) = \frac{\mathbf{r}^2}{48S_0}\left[16S_0S_2 - \mathbf{r}^2(\nabla S_1)^2\right], \tag{30}$$

$$T_5(\mathbf{r}) = \frac{(\mathbf{r}^2)^2}{96S_0^2}\left[-2S_0\nabla S_1\cdot\nabla S_2 + S_1(\nabla S_1)^2\right] + \frac{\mathbf{r}^2}{4}S_3. \tag{31}$$

In fact, we have a recursive formula for computing T_P for $P \geq 3$,

$$(P-1)S_0T_P = \sum_{k=1}^{P-2} S_k T_{P-k} - \frac{1}{4}\sum_{k=2}^{P-2} \nabla T_{k+1} \cdot \nabla T_{P-k+1}. \tag{32}$$

Then we use the truncated sum $\tilde{T}_P \equiv \sum_{\nu=2}^{P} T_\nu$ to approximate T near the source, and we further choose $\tilde{\tau}_P \equiv \sqrt{\tilde{T}_P}$ to approximate τ near the source with accuracy

$$|\tau(\mathbf{r}) - \tilde{\tau}_P(\mathbf{r})| = O(|\mathbf{r}|^P), \ |\mathbf{r}| \to 0.$$

Taking $\tilde{\tau}_P$ as high-order approximations of τ near the source, we apply high-order LxF-WENO methods to solve the factored eikonal equation as shown below.

3.2 High-Order Factorization of Coefficients v_s

Although v_s are assumed to be analytic near the source, we still need to obtain high-order approximations to v_s within a small neighborhood of the source so that high-order numerical schemes can be initialized near the source. Therefore, we will expand the coefficients v_s as homogeneous polynomials of degree k in $\mathbf{r}$ as well.

Similarly, the coefficient v_0 can be expanded as

$$v_0 = \sum_{k=0}^{\infty} B_k(\mathbf{r}), \tag{33}$$

where $B_k(\mathbf{r})$ are homogeneous polynomials of degree k in $\mathbf{r}$ and

$$B_0 = \frac{n_0^{m-2}}{2\pi^{(m-1)/2}}.$$

It follows that B_ν can be determined term by term by substituting (33) into (13) for $s = -1$:

$$\left(\sum_{\nu=2}^{\infty} \nabla T_\nu(\mathbf{r})\right)\cdot\left(\sum_{\nu=1}^{\infty} \nabla B_\nu(\mathbf{r})\right)+\left(\sum_{\nu=0}^{\infty} B_\nu(\mathbf{r})\right)\left[\frac{1}{2}\left(\sum_{\nu=2}^{\infty} \Delta T_\nu(\mathbf{r})\right) - m\left(\sum_{\nu=0}^{\infty} S_\nu(\mathbf{r})\right)\right] = 0. \tag{34}$$

Comparing the linear terms in (34) and using the homogeneity of B_1, we have

$$\begin{aligned} & \nabla T_2 \cdot \nabla B_1 + \frac{1}{2}(B_0\Delta T_3 + B_1 \Delta T_2) - m(B_0 S_1 + B_1 S_0) = 0, \\ \Rightarrow \ & 2S_0\mathbf{r}\cdot\nabla B_1 + \frac{1}{2}(B_0\Delta T_3 + 2B_1 m S_0) - m(B_0 S_1 + B_1 S_0) = 0, \\ \Rightarrow \ & 2S_0 B_1 + \frac{1}{2}B_0\Delta T_3 - m B_0 S_1 = 0, \\ \Rightarrow \ & B_1 = \frac{1}{2S_0}\left(-\frac{1}{2}B_0\Delta T_3 + m B_0 S_1\right). \end{aligned} \tag{35}$$

A recursive formula for B_P with $P \geq 2$ is given as

$$2PS_0B_P = -\sum_{k=1}^{P-1} \nabla B_k \cdot \nabla T_{P+2-k} - \frac{1}{2}\sum_{k=0}^{P-1} B_k \Delta T_{P+2-k} + m\sum_{k=0}^{P-1} B_k S_{P-k}. \tag{36}$$

Consequently, we can now use the truncated sum to approximate v_0, i.e.,

$$\tilde{B}_P \equiv \sum_{k=0}^{P} B_k, \tag{37}$$

and

$$|\tilde{B}_P - v_0| = O(|\mathbf{r}|^P), \ |\mathbf{r}| \to 0.$$

Taking $\tilde{B}_P$ as high-order approximations of v_0 near the source, we will apply high-order LxF-WENO methods to solve the Babich's transport equation (13) for v_0 when $s = -1$.

The governing equation for the coefficient v_1 satisfies

$$\nabla\tau^2 \cdot \nabla v_1 + v_1 \left[\frac{\Delta\tau^2}{2} + n^2(2-m) \right] = \frac{\Delta v_0}{2}. \tag{38}$$

Near the source, we expand v_1 as

$$v_1 = \sum_{k=0}^{\infty} C_k(\mathbf{r}). \tag{39}$$

where C_0 is the initial value of v_1 at the source.

By substituting (39) into (38), we have

$$\begin{aligned} &\left(\sum_{k=2}^{\infty} \nabla T_k\right) \cdot \left(\sum_{k=1}^{\infty} \nabla C_k\right) + \left[\frac{1}{2}\left(\sum_{k=2}^{\infty} \Delta T_k\right) + (2-m)\left(\sum_{k=0}^{\infty} S_k\right)\right]\left(\sum_{k=1}^{\infty} C_k\right) \\ &\quad = \frac{1}{2}\left(\sum_{k=2}^{\infty} \Delta B_k\right). \end{aligned} \tag{40}$$

Comparing the zeroth-order terms in (40), we have

$$\begin{aligned} &\frac{1}{2}\Delta T_2 \ C_0 + (2-m) S_0 \ C_0 = \frac{1}{2}\Delta B_2, \\ &2 S_0 C_0 = \frac{1}{2}\Delta B_2. \end{aligned} \tag{41}$$

Comparing the linear terms in $\mathbf{r}$ in (40) and using the homogeneity of C_1, we have

$$\begin{aligned} &\nabla T_2 \cdot \nabla C_1 + \frac{1}{2}[\Delta T_2 \ C_1 + \Delta T_3 \ C_0] + (2-m)[S_0 \ C_1 + S_1 \ C_0] = \frac{1}{2}\Delta B_3, \\ &4 S_0 C_1 = \frac{1}{2}\Delta B_3 - \frac{1}{2}\Delta T_3 \ C_0 - (2-m) S_1 \ C_0. \end{aligned} \tag{42}$$

In general, the coefficient C_P for $P \geq 2$ can be obtained by comparing the Pth-order terms in (40):

$$\begin{aligned} &\sum_{k=1}^{P} \nabla C_k \cdot \nabla T_{P+2-k} + \frac{1}{2}\sum_{k=0}^{P} C_k \Delta T_{P+2-k} + (2-m)\sum_{k=0}^{P} C_k S_{P-k} = \frac{1}{2}\Delta B_{p+2}, \\ &2(P+1) S_0 C_P = \frac{1}{2}\Delta B_{p+2} - \sum_{k=1}^{P-1} \nabla C_k \cdot \nabla T_{P+2-k} - \frac{1}{2}\sum_{k=0}^{P-1} C_k \Delta T_{P+2-k} \\ &-(2-m)\sum_{k=0}^{P-1} C_k S_{P-k}. \end{aligned} \tag{43}$$

Consequently, we can now use the truncated sum to approximate v_1, i.e.,

$$\tilde{C}_P \equiv \sum_{k=0}^{P} C_k, \tag{44}$$

and

$$|\tilde{C}_P - v_1| = O(|\mathbf{r}|^P), \ |\mathbf{r}| \to 0.$$

Taking $\tilde{C}_P$ as high-order approximations of v_1 near the source, we will apply high-order LxF-WENO methods to solve the Babich's transport equation (13) for v_1 when $s = 0$.

Analogously, we can apply the above approach to derive high-order approximations of v_s near the source for $s \geq 1$, and here we will not pursue this further.

4 High-Order Lax–Friedrichs WENO Schemes

4.1 Schemes for Phase τ

We first recall a factorization approach to resolving the source singularity for computing τ [7,12,13,15,16,19,26]. In the factorization approach, τ is factored as

$$\tau = \tilde{\tau}\bar{\tau}, \tag{45}$$

where $\tilde{\tau}$ is pre-determined analytically to capture the source singularity such that $\bar{\tau}$ is the new unknown that is smooth at the source and satisfies the factored eikonal equation,

$$|\tilde{\tau}\nabla\bar{\tau} + \bar{\tau}\nabla\tilde{\tau}| = n(\mathbf{r}). \tag{46}$$

For instance, $\tilde{\tau}$ may be taken as $\tilde{\tau}(\mathbf{r}; \mathbf{r}_0) = n(\mathbf{r}_0)|\mathbf{r} - \mathbf{r}_0|$.

Since $\bar{\tau}$ is smooth at the source, we can solve Eq. (46) efficiently with high-order Lax–Friedrichs weighted essentially non-oscillatory (LxF-WENO) schemes as designed in [12,15,16,25,27], and these schemes in turn are built upon the first-order Lax–Friedrichs sweeping method [10]. In a P-th order LxF-WENO finite difference method on a mesh of size h, $\bar{\tau}$ must be initialized in a neighborhood of size $2(P-1)h$ centered at the source, and these initial values are fixed during iterations.

In the P-th order LxF-WENO method for solving (46) to obtain $\bar{\tau}$, we first choose $\tilde{\tau}(\mathbf{r}) \equiv \sqrt{S_0}|\mathbf{r}|$. To initialize $\bar{\tau}$ near the source, $\bar{\tau}$ is assigned as 1 at the source and as $\tilde{\tau}_P/\tilde{\tau}$ at other points in the $2(P-1)h$ neighborhood of the source so that these values are fixed during the LxF-WENO sweeping iterations. At other points, the LxF-WENO iterations are used to update $\bar{\tau}$ with $\tilde{\tau}(\mathbf{r}) \equiv \sqrt{S_0}|\mathbf{r}|$. In the following, we will take $P = 6$ for computing τ.

4.2 Schemes for Coefficients v_s

In the P-th order LxF-WENO method for solving transport equations (13) when $s = -1$, v_0 is assigned as $\tilde{B}_P$ in the $2(P-1)h$-neighborhood of the source so that these values are fixed during the LxF-WENO iterations; at other points, the LxF-WENO iterations are used to update v_0.

Similarly, when $s = 0$, v_1 is assigned as $\tilde{C}_P$ in the $2(P-1)h$-neighborhood of the source so that these values are fixed during the LxF-WENO iterations; at other points, the LxF-WENO iterations are used to update v_1.

4.3 3rd- and 5th-Order WENO LxF Schemes

Since both Eqs. (46) and (13) are first-order scalar hyperbolic equations, we summarize the high-order Lax–Friedrichs schemes for these equations as follows. We consider the general Hamilton–Jacobi equation:

$$F(x, y, u, u_x, u_y) = f(x, y), \tag{47}$$

where F is convex in the gradient variable.

Let u_{ij} denote the value of u at grid point (x_i, y_j) and h be the step size in both directions. At a generic grid point $(i, j) = (x_i, y_j)$ with neighbors

$$N\{i, j\} = \{(x_{i-1}, y_j), (x_{i+1}, y_j), (x_i, y_{j-1}), (x_i, y_{j+1})\}, \tag{48}$$

we consider the Lax–Friedrichs Hamiltonian:

$$\begin{aligned} F^{LF}(x_i, y_j, u_{i,j}, u_{N\{i,j\}}) &= F\left(x_i, y_j, u_{i,j}, \frac{u_{i+1,j} - u_{i-1,j}}{2h}, \frac{u_{i,j+1} - u_{i,j-1}}{2h}\right) \\ &\quad -\alpha_x \frac{u_{i+1,j} - 2u_{ij} + u_{i-1,j}}{2h} - \alpha_y \frac{u_{i,j+1} - 2u_{ij} + u_{i,j-1}}{2h}, \end{aligned} \tag{49}$$

where α_x and α_y are chosen such that for a fixed (x_i, y_j),

$$\frac{\partial F^{LF}}{\partial u_{ij}} \geq 0, \quad \text{and} \quad \frac{\partial F^{LF}}{\partial u_{N\{i,j\}}} \leq 0.$$

For example, we can choose

$$\alpha_x = \max_{m \leq u \leq M, A \leq p \leq B, C \leq q \leq D} \left\{ |F_1(x, y, u, p, q)| + \frac{h}{2} |\frac{\partial F}{\partial u}(x, y, u, p, q)| \right\}, \tag{50}$$

$$\alpha_y = \max_{m \leq u \leq M, A \leq p \leq B, C \leq q \leq D} \left\{ |F_2(x, y, u, p, q)| + \frac{h}{2} |\frac{\partial F}{\partial u}(x, y, u, p, q)| \right\}, \tag{51}$$

where F_1 and F_2 denote the derivatives of the F with respect to the first and the second gradient component, respectively. The flux F^{LF} is monotone for $m \leq u_{ij} \leq M$, $A \leq p \leq B$, and $C \leq q \leq D$ with $p = (u_{i+1,j} - u_{i-1,j})/2h$ and $q = (u_{i,j+1} - u_{i,j-1})/2h$.

The first-order Lax–Friedrichs scheme is [10]

$$\begin{aligned} u_{i,j}^{new} &= \left(\frac{1}{\alpha_x/h + \alpha_y/h}\right)\left[f_{i,j} - F\left(x_i, y_j, u_{i,j}^{old}, \frac{u_{i+1,j} - u_{i-1,j}}{2h}, \frac{u_{i,j+1} - u_{i,j-1}}{2h}\right)\right. \\ &\quad \left. + \alpha_x \frac{u_{i+1,j} + u_{i-1,j}}{2h} + \alpha_y \frac{u_{i,j+1} + u_{i,j-1}}{2h}\right]. \end{aligned} \tag{52}$$

The third-order WENO Lax–Friedrichs scheme can be obtained by replacing $u_{i-1,j}$, $u_{i+1,j}$, $u_{i,j-1}$, and $u_{i,j+1}$ in (52) with the following approximations [27],

$$\begin{aligned} u_{i-1,j} &= u_{i,j} - h(u_x)^-_{i,j}, \quad u_{i+1,j} = u_{i,j} + h(u_x)^+_{i,j}, \\ u_{i,j-1} &= u_{i,j} - h(u_y)^-_{i,j}, \quad u_{i,j+1} = u_{i,j} + h(u_y)^+_{i,j}, \end{aligned} \tag{53}$$

where $(u_x)^-_{i,j}$ and $(u_x)^+_{i,j}$ are the third-order WENO approximations of u_x, and $(u_y)^-_{i,j}$ and $(u_y)^+_{i,j}$ are the third-order WENO approximations of u_y as defined in [8].

Similar to [10,25,27], the fifth-order WENO Lax–Friedrichs scheme can be obtained by replacing $u_{i-1,j}$, $u_{i+1,j}$, $u_{i,j-1}$ and $u_{i,j+1}$ in (52) with those formulas in (53), where $(u_x)^-_{i,j}$

and $(u_x)^+_{i,j}$ are the fifth-order WENO approximations of u_x, and $(u_y)^-_{i,j}$ and $(u_y)^+_{i,j}$ are the fifth-order WENO approximations of u_y as defined in [8].

5 Convergence of WENO LxF Schemes

In this section, we consider the two dimensional static Hamilton–Jacobi equation

$$F(x, z, u, u_x, u_z) = f(x, z), \tag{54}$$

and the WENO based Lax–Friedrichs scheme is

$$u^{new}_{i,j} = \frac{h}{\alpha_x + \alpha_z}\left[f_{i,j} - F\left(x_i, z_j, u^{old}_{i,j}, \frac{u_{i+1,j} - u_{i-1,j}}{2h}, \frac{u_{i,j+1} - u_{i,j-1}}{2h}\right) + \alpha_x \frac{u_{i+1,j} + u_{i-1,j}}{2h} + \alpha_z \frac{u_{i,j+1} + u_{i,j-1}}{2h}\right] \tag{55}$$

where h represents the spatial partition and

$$\begin{aligned} u_{i-1,j} &= u_{i,j} - h(u_x)^-_{i,j}; \qquad u_{i+1,j} = u_{i,j} + h(u_x)^+_{i,j}; \\ u_{i,j-1} &= u_{i,j} - h(u_z)^-_{i,j}; \qquad u_{i,j+1} = u_{i,j} + h(u_z)^+_{i,j}. \end{aligned} \tag{56}$$

Here $(u_x)^-_{i,j}$ and $(u_x)^+_{i,j}$ are WENO approximations of u_x; $(u_z)^-_{i,j}$ and $(u_z)^+_{i,j}$ are WENO approximations of u_z.

Theorem 5.1 *The p-th order WENO based Lax–Friedrichs sweeping scheme* (55)–(56) *for the static Hamilton–Jacobi equation* (54) *yields p-th order accuracy when u, F and f are smooth.*

The proof of Theorem 5.1 follows from the following two lemmas.

Lemma 5.2 *Assume that $u^*(x, z)$ is the solution to the static Hamilton–Jacobi equation* (54)*, and $u^*(x, z, T)$ is the solution to the time-dependent Hamilton–Jacobi equation* (57) *at time T,*

$$u_t + F(x, z, u, u_x, u_z) = f(x, z) \tag{57}$$

then $\| u^*(x, z) - u^*(x, z, T) \|_\infty \to 0$ as $T \to \infty$.

This is obvious since the static Hamilton–Jacobi equation (54) can be considered as the steady state solution of the time dependent Hamilton–Jacobi equation (57) [6,11,25]. We can follow the method of lines to numerically solve (57). For example we first apply high order WENO schemes for spatial discretization and then use Runge–Kutta methods for temporal discretization. One the other hand, the convergence of nonlinear Jacobi iteration implies the convergence of the Gauss–Seidel iteration under suitable conditions on the Jacobian matrices of the iteration operators [5,18,21]. In fact, it can be proved that the spectral radius of the Jacobian of Gauss–Seidel iterative procedure is smaller than the spectral radius of the corresponding Jacobi iteration if the latter is smaller than one [18]. Thus Gauss–Seidel procedure enjoys better convergence than its Jacobi counterpart. Therefore, to show the convergence of the scheme (55)–(56) for (54), we only need to prove the the convergence of WENO and Runge–Kutta methods for time-dependent Hamilton–Jacobi equation since the time marching approach is one type of Jacobi iterations.

Lemma 5.3 *Assume that $u^*(x,z,T)$ and $u_h(x,z,T)$ are the exact and numerical solution to the time dependent Hamilton–Jacobi equation (57) at time T obtained via p-th order WENO scheme with Lax–Friedrichs flux and n-th ($n \geq \max(p,3)$) order Runge–Kutta time discretization scheme, and u, F and f have $p+q_0+4$ continuous derivatives in the domain of dependence of (x,z,t) as defined in [22]. Under an appropriate chosen CFL condition, we have*

$$\|u^*(x,z,T) - u_h(x,z,T)\|_\infty \sim O(h^p), \tag{58}$$

where q_0 is a small integer related to the smoothness of the fully discrete operator [22].

Proof Without loss of generality, we assume that $p = 5$. The consistent WENO based Lax–Friedrichs sweeping operator for the time dependent Hamilton–Jacobi equation (57) is

$$\begin{aligned} L = \frac{h}{\alpha_x + \alpha_z}\Bigg[& f_{i,j} - F\left(x_i, z_j, u_{i,j}, \frac{u_{i+1,j} - u_{i-1,j}}{2h}, \frac{u_{i,j+1} - u_{i,j-1}}{2\Delta x}\right) \\ & + \alpha_x \frac{u_{i+1,j} + u_{i-1,j}}{2h} + \alpha_z \frac{u_{i,j+1} + u_{i,j-1}}{2h}\Bigg] - u_{i,j} \end{aligned} \tag{59}$$

where $u_{i-1,j}$, $u_{i+1,j}$, $u_{i,j-1}$ and $u_{i,j+1}$ are defined as in (56). $(u_x)^-_{i,j}$, $(u_x)^+_{i,j}$, $(u_z)^-_{i,j}$, $(u_z)^+_{i,j}$ are the 5-th order WENO biased approximations of u_x and u_z, respectively. It's easy to see that the stencil for the operator L is

$$\begin{aligned} & \{u_{i,j}, u_{i-3,j}, u_{i-2,j}, u_{i-1,j}, u_{i+1,j}, u_{i+2,j}, u_{i+3,j}, u_{i,j-3}, u_{i,j-2}, u_{i,j-1}, \\ & u_{i,j+1}, u_{i,j+2}, u_{i,j+3}\}. \end{aligned} \tag{60}$$

The WENO based Lax–Friedrichs sweeping scheme is smooth in the sense that the spatial operator L is infinitely differentiable with respect to any of its arguments. Strang's theorem [22] implies that the scheme is convergent if its first variation is l_2-stable. We are going to prove the l_2 stability of the first variation of the 5-th order WENO operator in the following.

The first variation $\widetilde{L}$ is defined as

$$\widetilde{L} \equiv \sum_{k=i-3}^{i+3} \sum_{l=j-3}^{j+3} \frac{\partial L}{\partial u_{k,l}}(u_{i,j}, \ldots, u_{i,j}) u_{k,l} \tag{61}$$

Since the solution is assumed to be smooth, the 5-th order WENO approximation is equivalent to the upstream central approximation [9], i.e.

$$\begin{aligned} (u_x)^-_{i,j} &= -\frac{1}{30h}u_{i-3,j} + \frac{1}{4h}u_{i-2,j} - \frac{1}{h}u_{i-1,j} + \frac{1}{3h}u_{i,j} + \frac{1}{2h}u_{i+1,j} - \frac{1}{20h}u_{i+2,j}; \\ (u_x)^+_{i,j} &= \frac{1}{30h}u_{i+3,j} - \frac{1}{4h}u_{i+2,j} + \frac{1}{h}u_{i+1,j} - \frac{1}{3h}u_{i,j} - \frac{1}{2h}u_{i-1,j} + \frac{1}{20h}u_{i-2,j}, \end{aligned} \tag{62}$$

and

$$\begin{aligned} (u_z)^-_{i,j} &= -\frac{1}{30h}u_{i,j-3} + \frac{1}{4h}u_{i,j-2} - \frac{1}{h}u_{i,j-1} + \frac{1}{3h}u_{i,j} + \frac{1}{2h}u_{i,j+1} - \frac{1}{20h}u_{i,j+2}; \\ (u_z)^+_{i,j} &= \frac{1}{30h}u_{i,j+3} - \frac{1}{4h}u_{i,j+2} + \frac{1}{h}u_{i,j+2} - \frac{1}{3h}u_{i,j} - \frac{1}{2h}u_{i,j-1} + \frac{1}{20h}u_{i,j-2}. \end{aligned} \tag{63}$$

With these WENO expressions, the 4-th and 5-th arguments of F can be replaced by

$$u_x \approx \frac{u_{i+1,j} - u_{i-1,j}}{2h} \tag{64}$$

$$\approx \frac{1}{2}\left((u_x)^+_{i,j} + (u_x)^-_{i,j}\right)$$

$$= \frac{1}{h}\left[-\frac{1}{60}u_{i-3,j} + \frac{3}{20}u_{i-2,j} - \frac{3}{4}u_{i-1,j} + \frac{3}{4}u_{i+1,j} - \frac{3}{20}u_{i+2,j} + \frac{1}{60}u_{i+3,j}\right]; \tag{65}$$

$$u_z \approx \frac{u_{i,j+1} - u_{i,j-1}}{2h} \tag{66}$$

$$\approx \frac{1}{2}\left((u_z)^+_{i,j} + (u_z)^-_{i,j}\right)$$

$$= \frac{1}{h}\left[-\frac{1}{60}u_{i,j-3} + \frac{3}{20}u_{i,j-2} - \frac{3}{4}u_{i,j-1} + \frac{3}{4}u_{i,j+1} - \frac{3}{20}u_{i,j+2} + \frac{1}{60}u_{i,j+3}\right]. \tag{67}$$

Also

$$\frac{u_{i+1,j} + u_{i-1,j}}{2h} \approx \frac{1}{h}\left[\frac{1}{60}u_{i+3,j} - \frac{1}{10}u_{i+2,j} + \frac{1}{4}u_{i+1,j} + \frac{2}{3}u_{i,j} + \frac{1}{4}u_{i-1,j} - \frac{1}{10}u_{i-2,j} + \frac{1}{60}u_{i-3,j}\right];$$

$$\frac{u_{i,j+1} + u_{i,j-1}}{2h} \approx \frac{1}{h}\left[\frac{1}{60}u_{i,j+3} - \frac{1}{10}u_{i,j+2} + \frac{1}{4}u_{i,j+1} + \frac{2}{3}u_{i,j} + \frac{1}{4}u_{i,j-1} - \frac{1}{10}u_{i,j-2} + \frac{1}{60}u_{i,j-3}\right]. \tag{68}$$

After some calculations, the first variation $\widetilde{L}$ is

$$\begin{aligned}
\widetilde{L} = &-\frac{h}{\alpha_x+\alpha_z}\frac{\partial F}{\partial u}u_{i,j} + \frac{1}{\alpha_x+\alpha_z}\left[-\frac{1}{3}\alpha_x - \frac{1}{3}\alpha_z\right]u_{i,j} \\
&+ \frac{1}{\alpha_x+\alpha_z}\left[-\frac{\partial F}{\partial u_x}\left(-\frac{1}{60}\right)+\frac{1}{60}\alpha_x\right]u_{i-3,j} + \frac{1}{\alpha_x+\alpha_z}\left[-\frac{\partial F}{\partial u_x}\left(\frac{3}{20}\right)-\frac{1}{10}\alpha_x\right]u_{i-2,j} \\
&+ \frac{1}{\alpha_x+\alpha_z}\left[-\frac{\partial F}{\partial u_x}\left(-\frac{3}{4}\right)+\frac{1}{4}\alpha_x\right]u_{i-1,j} + \frac{1}{\alpha_x+\alpha_z}\left[-\frac{\partial F}{\partial u_x}\left(\frac{3}{4}\right)+\frac{1}{4}\alpha_x\right]u_{i+1,j} \\
&+ \frac{1}{\alpha_x+\alpha_z}\left[-\frac{\partial F}{\partial u_x}\left(-\frac{3}{20}\right)-\frac{1}{10}\alpha_x\right]u_{i+2,j} + \frac{1}{\alpha_x+\alpha_z}\left[-\frac{\partial F}{\partial u_x}\left(\frac{1}{60}\right)+\frac{1}{60}\alpha_x\right]u_{i+3,j} \\
&+ \frac{1}{\alpha_x+\alpha_z}\left[-\frac{\partial F}{\partial u_z}\left(-\frac{1}{60}\right)+\frac{1}{60}\alpha_z\right]u_{i,j-3} + \frac{1}{\alpha_x+\alpha_z}\left[-\frac{\partial F}{\partial u_z}\left(\frac{3}{20}\right)-\frac{1}{10}\alpha_z\right]u_{i,j-2} \\
&+ \frac{1}{\alpha_x+\alpha_z}\left[-\frac{\partial F}{\partial u_z}\left(-\frac{3}{4}\right)+\frac{1}{4}\alpha_z\right]u_{i,j-1} + \frac{1}{\alpha_x+\alpha_z}\left[-\frac{\partial F}{\partial u_z}\left(\frac{3}{4}\right)+\frac{1}{4}\alpha_z\right]u_{i,j+1} \\
&+ \frac{1}{\alpha_x+\alpha_z}\left[-\frac{\partial F}{\partial u_z}\left(-\frac{3}{20}\right)-\frac{1}{10}\alpha_z\right]u_{i,j+2} + \frac{1}{\alpha_x+\alpha_z}\left[-\frac{\partial F}{\partial u_z}\left(\frac{1}{60}\right)+\frac{1}{60}\alpha_z\right]u_{i,j+3}
\end{aligned} \tag{69}$$

which can be rewritten as

$$\widetilde{L} = -\frac{h}{\alpha_x+\alpha_z}\frac{\partial F}{\partial u}u_{i,j} + \frac{1}{\alpha_x+\alpha_z}\left(\mathrm{T1}+\mathrm{T2}\right), \tag{70}$$

where

$$\begin{aligned}
\mathrm{T1} = &-\frac{\partial F}{\partial u_x}\left[-\frac{1}{60}u_{i-3,j}+\frac{3}{20}u_{i-2,j}-\frac{3}{4}u_{i-1,j}+\frac{3}{4}u_{i+1,j}-\frac{3}{20}u_{i+2,j}+\frac{1}{60}u_{i+3,j}\right]\\
&+\alpha_x\left[-\frac{1}{60}u_{i-3,j}+\frac{1}{15}u_{i-2,j}-\frac{1}{12}u_{i-1,j}+\frac{1}{12}u_{i+1,j}-\frac{1}{15}u_{i+2,j}+\frac{1}{60}u_{i+3,j}\right]\\
&-\alpha_x\left[-\frac{1}{30}u_{i-3,j}+\frac{1}{6}u_{i-2,j}-\frac{1}{3}u_{i-1,j}+\frac{1}{3}u_{i,j}-\frac{1}{6}u_{i+1,j}+\frac{1}{30}u_{i+2,j}\right], \qquad (71)\\
\mathrm{T2} = &-\frac{\partial F}{\partial u_z}\left[-\frac{1}{60}u_{i,j-3}+\frac{3}{20}u_{i,j-2}-\frac{3}{4}u_{i,j-1}+\frac{3}{4}u_{i,j+1}-\frac{3}{20}u_{i,j+2}+\frac{1}{60}u_{i,j+3}\right]\\
&+\alpha_z\left[-\frac{1}{60}u_{i,j-3}+\frac{1}{15}u_{i,j-2}-\frac{1}{12}u_{i,j-1}+\frac{1}{12}u_{i,j+1}-\frac{1}{15}u_{i,j+2}+\frac{1}{60}u_{i,j+3}\right]\\
&-\alpha_z\left[-\frac{1}{30}u_{i,j-3}+\frac{1}{6}u_{i,j-2}-\frac{1}{3}u_{i,j-1}+\frac{1}{3}u_{i,j}-\frac{1}{6}u_{i,j+1}+\frac{1}{30}u_{i,j+2}\right]. \qquad (72)
\end{aligned}$$

Applying the classical Fourier analysis to $\widetilde{L}$ in (70), we see that the first two terms in T1 and T2 render purely imaginary spectrum, while the last term is a 5-th order upwind-biased difference, which has a spectrum of the form

$$\frac{16}{15}\left(\sin\left(\frac{\theta}{2}\right)\right)^5\left(\sin\left(\frac{\theta}{2}\right)+i\cos\left(\frac{\theta}{2}\right)\right) \qquad (73)$$

where $0 \le \theta \le 2\pi$.

By the assumption $\frac{\partial F^{LF}}{\partial u_{i,j}} \ge 0$, we can obtain

$$\frac{\partial F}{\partial u}-\frac{2}{3h}(\alpha_x+\alpha_z) \ge 0, \qquad (74)$$

with α_x, α_z and h positive. Therefore $\frac{\partial F}{\partial u} \ge 0$.

We conclude that the spectrum of the operator $\widetilde{L}$ lies fully on the left half of the complex plane, leading to the l_2 stability which further implies the convergence of the scheme.

6 Numerical Examples

We will carry out some numerical experiments to verify that Babich's expansion based high-order Eulerian asymptotics constructed by solving eikonal and transport equations directly provides valid, efficient and accurate asymptotic solutions for point-source Helmholtz equations in the high frequency regime before caustics occur. Although we exclude the situation of caustics, the schemes developed here for solving eikonal and transport equations can be incorporated into some recent methods, such as fast Huygens sweeping methods to treat caustics [14].

We will compare the first-order and second-order Babich's expansions carefully. By the first-order expansion, we mean that we will keep only the leading-order term in (6); by the second-order expansion, we mean that we will keep the first two terms only, namely, $s = 0, 1$, in (6).

In numerical implementations, to obtain the second coefficient v_1 with first-order accuracy, we need to compute the first coefficient v_0 with at least third-order accuracy, implying that the phase τ be computed at least with fifth-order accuracy. The fifth-order accurate τ can

be obtained by using the fifth-order Lax–Friedrichs WENO scheme and the fifth-order factorization around the source. The first amplitude coefficient v_0 can be calculated by solving Eq. (13) with $s = -1$ with the third-order Lax–Friedrichs WENO scheme. When solving Eq. (13), we need to compute $\nabla\tau^2$ and $\Delta\tau$; we use the third-order WENO to compute $\nabla\tau^2$ and a fourth-order finite-difference method to compute $\Delta\tau^2$ except for points around the source, while the approximate analytic expression of τ is used to compute $\nabla\tau^2$ and $\Delta\tau^2$ at those points around the source. Since τ is of fifth-order accuracy, $\nabla\tau^2$ and $\Delta\tau^2$ will be of third-order accuracy. Therefore, v_0 will also be of third-order accuracy. After v_0 is computed, Δv_0 is computed by the fourth-order finite-difference scheme. Finally, v_1 is obtained by solving the transport equation (13) with $s = 0$ by the third-order Lax–Friedrichs WENO scheme.

As for boundary conditions in solving eikonal and transport equations, we use high-order extrapolation to naturally extend interior values beyond the boundary. One may apply more elegant boundary conditions as designed in [25] to treat the equations presented here, but we are not pursuing this further in the current work.

In the following, we use w_0 and w_1 to denote the first and second term of Babich's expression (6), respectively; w_0 and $w = w_0 + w_1$ are the first-order and second-order Babich's asymptotic solution, respectively.

To obtain the direct solution for the point-source Helmholtz equation, we first solve the corresponding time-domain wave equation by a finite-difference time-domain (FDTD) method and then Fourier-integrate in time to obtain the frequency-domain solution for the Helmholtz equation.

6.1 2-D Examples

In the following 2-D examples, the phase τ is computed by the fifth-order Lax–Friedrichs WENO scheme with the sixth-order ($P = 6$) factorization around the source.

v_0 is computed by the third-order Lax–Friedrichs WENO scheme with the third-order ($P = 3$) factorization around the source. v_1 is computed by the third-order Lax–Friedrichs WENO scheme with the first-order ($P = 1$) factorization around the source.

The FDTD results are computed in the domain $[-0.2, 1.2]^2$ with mesh grid 701×701 for both $\omega = \pi$ and $\omega = 8\pi$.

Example 1 **a 2-D constant refractive index** The computational setup is the following.

- The refractive index $n(x, y) = 2$;
- The computational domain is $[0, 1] \times [0, 1]$;
- The mesh size is 100×100 with the grid size $h = 0.01$;
- The angular frequency $\omega = \pi$ or 8π.
- The source point is $(0.5, 0.5)$.

Figure 1 shows the errors of τ^2, $\frac{\partial}{\partial x}\tau^2$ and $\frac{\partial^2}{\partial x^2}\tau^2$, as τ^2 rather than τ is the most important quantity in the Babich's transport equations. Figure 2 shows the error of v_0 along with the fields of Δv_0 and v_1.

Figures 3 and 4 show the real part of w_0, $w = w_0 + w_1$, and the exact solution w_{exact} at $x = 0.2, x = 0.5$ and $x = 0.6$ with $\omega = \pi$ and $\omega = 8\pi$, respectively. As we can see, the three solutions match with each other very well.

Example 2 **Constant gradient case for** $\frac{1}{n}$ The computational setup is the following.

- The refractive index $n(x, y) = \dfrac{1}{0.5 - 0.5 * (y - 0.5)}$;

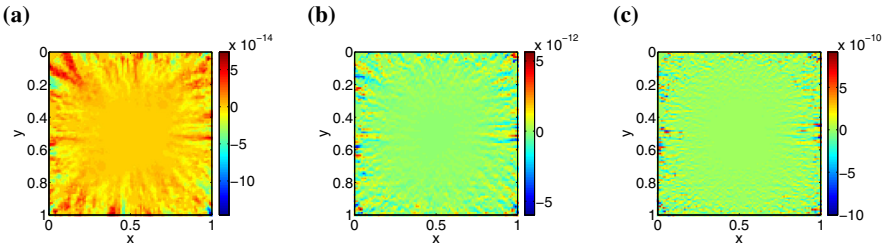

Fig. 1 Example 1: **a** The error of τ^2. **b** The error of $\frac{\partial}{\partial x}\tau^2$. **c** The error of $\frac{\partial^2}{\partial x^2}\tau^2$.

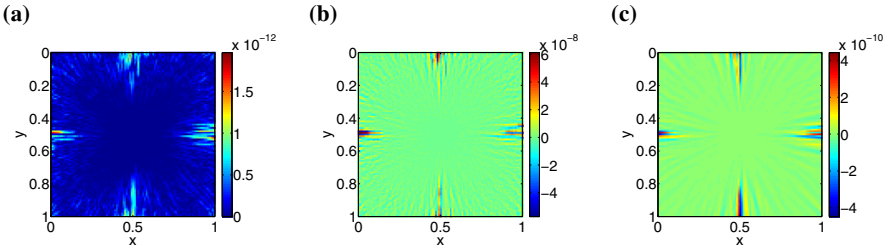

Fig. 2 Example 1: **a** The error of v_0. **b** The field of Δv_0. **c** The field of v_1

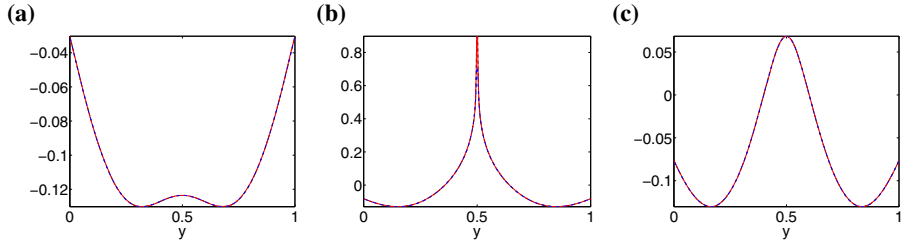

Fig. 3 Example 1: The real part of w_0, w and w_{exact} at **a** $x = 0.2$, **b** $x = 0.5$, and **c** $x = 0.6$ with $\omega = \pi$. *Black dashed line* for w_0, *red solid line* for w, and *blue dash-dot line* for w_{exact} (Color figure online)

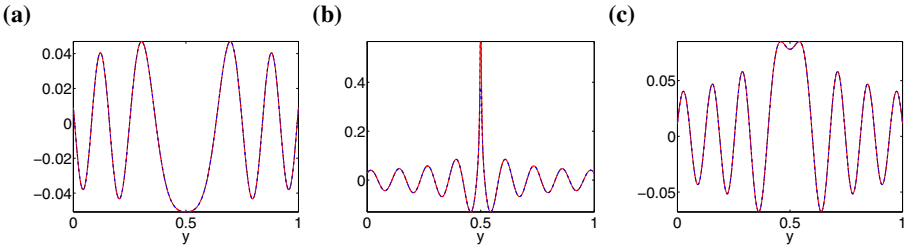

Fig. 4 Example 1: The real part of w_0, w and w_{exact} at **a** $x = 0.2$, **b** $x = 0.5$, and **c** $x = 0.6$ with $\omega = 8\pi$. *Black dashed line* for w_0, *red solid line* for w, and *blue dash-dot line* for w_{exact} (Color figure online)

- The computational domain is $[0, 1] \times [0, 1]$;
- The mesh size is 100×100 with the grid size $h = 0.01$;
- The angular frequency $\omega = \pi$ or 8π.
- The source point is $(0.5, 0.5)$.

Table 1 Example 2: The l_∞ and l_1 errors of τ and it's order of convergence

Mesh	101×101	201×201	401×401	801×801
l_∞	6.00×10^{-8}	1.88×10^{-9}	5.61×10^{-11}	1.74×10^{-12}
Order		5.00	5.07	5.01
l_1	6.37×10^{-9}	1.65×10^{-10}	4.46×10^{-12}	1.32×10^{-13}
Order		5.27	5.21	5.08
♯ Iter	212	363	653	1237
CPU time (s)	1.96	14.63	109.49	822.08

The phase τ is computed by the hybrid schemes with fifth-order multiplicative factorization and the fifth-order Lax–Friedrichs scheme

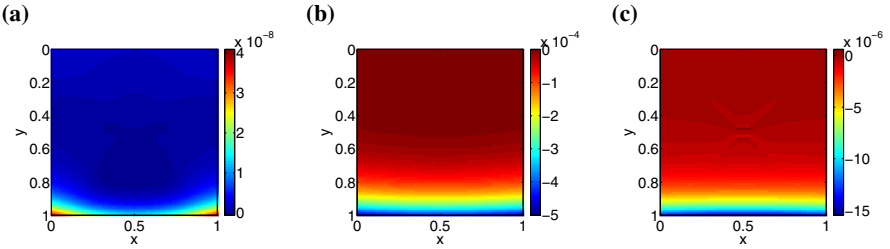

Fig. 5 Example 2: **a** The error of τ^2. **b** The error of $\frac{\partial}{\partial x}\tau^2$. **c** The error of $\frac{\partial^2}{\partial x^2}\tau^2$.

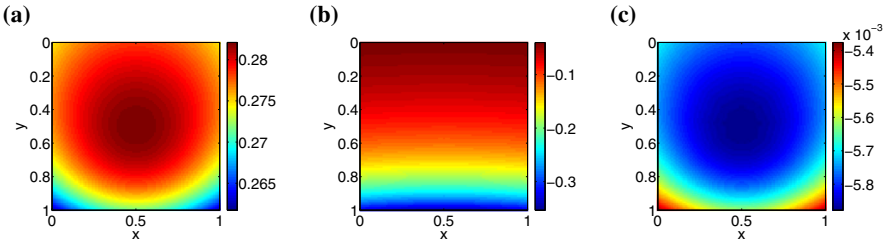

Fig. 6 Example 2: **a** The field of v_0. **b** The field of Δv_0. **c** The field of v_1.

In this case, the exact solution for the phase τ can be computed.

To validate that our method is fifth-order accurate for computing phase τ, we have computed the order of convergence as shown in Table 1, which indicates the fifth-order convergence in both l_1 and l_∞ norms.

Figure 5 shows the errors of τ^2, $\frac{\partial}{\partial x}\tau^2$ and $\frac{\partial^2}{\partial x^2}\tau^2$. Figure 6 shows the field of v_0 along with the fields of Δv_0 and v_1.

Next we compare our asymptotic solutions with the direct result obtained by solving the Helmholtz equation. Figure 7 shows the real part of w_0, w, and w_{FDTD} at $x = 0.2$, $x = 0.5$ and $x = 0.6$ with $\omega = \pi$. Figure 8 shows the results at $y = 0.2$, $y = 0.5$ and $y = 0.6$ with $\omega = \pi$. Figures 9 and 10 show the results for $\omega = 8\pi$. We can see that the asymptotic solution becomes more accurate as the large parameter ω increases.

Figures 11 and 12 show the wave field obtained by a direct method, the one-term expansion w_0, and the two-term expansion $w = w_0 + w_1$ with $\omega = \pi$ and 8π, respectively.

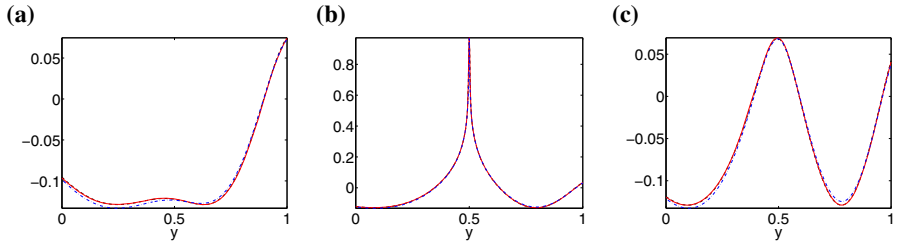

Fig. 7 Example 2: The real part of w_0, w and w_{exact} at **a** $x = 0.2$, **b** $x = 0.5$, and **c** $x = 0.6$ with $\omega = \pi$. *Black dashed line* for w_0, *red solid line* for w, and *blue dash-dot line* for w_{FDTD} (Color figure online)

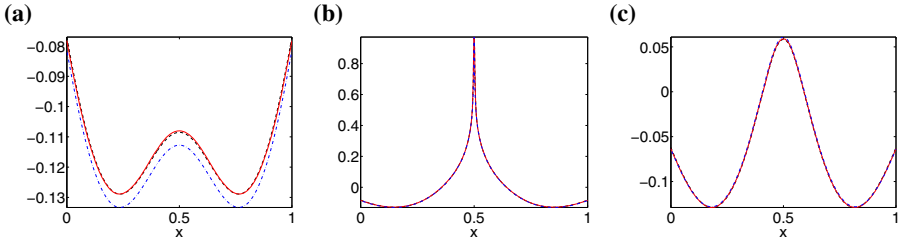

Fig. 8 Example 2: The real part of w_0, w and w_{exact} at **a** $y = 0.2$, **b** $y = 0.5$, and **c** $y = 0.6$ with $\omega = \pi$. *Black dashed line* for w_0, *red solid line* for w, and *blue dash-dot line* for w_{FDTD} (Color figure online)

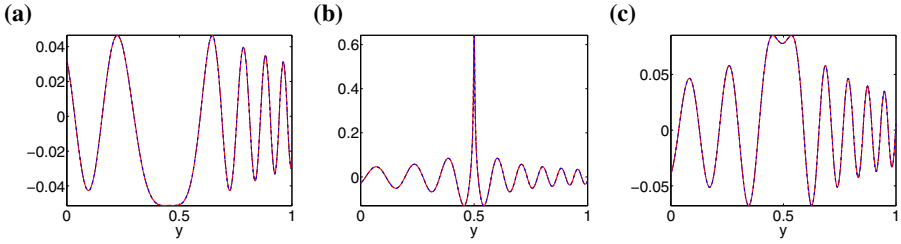

Fig. 9 Example 2: The real part of w_0, w and w_{exact} at **a** $x = 0.2$, **b** $x = 0.5$, and **c** $x = 0.6$ with $\omega = 8\pi$. *Black dashed line* for w_0, *red solid line* for w, and *blue dash-dot line* for w_{FDTD} (Color figure online)

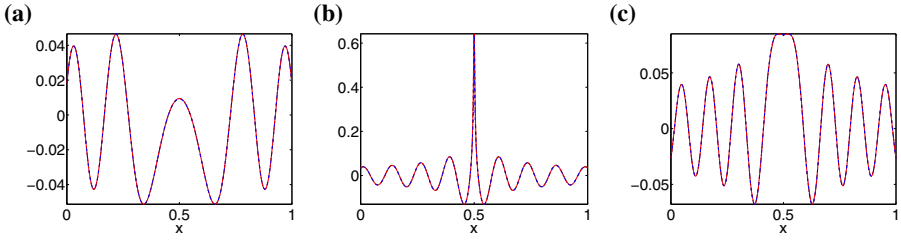

Fig. 10 Example 2: The real part of w_0, w and w_{FDTD} at **a** $y = 0.2$, **b** $y = 0.5$, and **c** $y = 0.6$ with $\omega = 8\pi$. *Black dashed line* for w_0, *red solid line* for w, and *blue dash-dot line* for w_{FDTD} (Color figure online)

6.2 3-D Examples

In the following 3-D examples, the phase τ is computed by the fifth-order Lax–Friedrichs WENO scheme with the sixth-order ($P = 6$) factorization around the source.

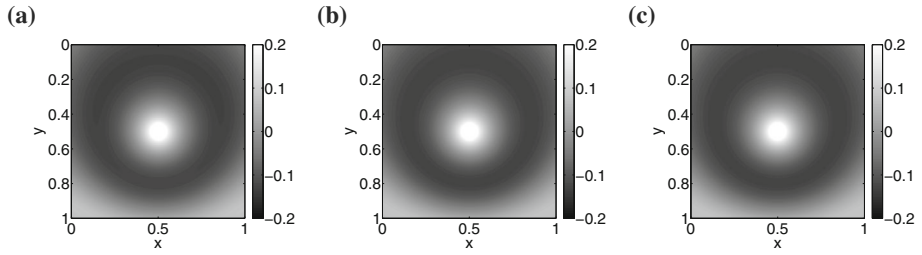

Fig. 11 Example 2: The wave field of **a** FDTD solution, **b** the one-term expansion w_0, and **c** the two-term expansion $w = w_0 + w_1$ with frequency $\omega = \pi$

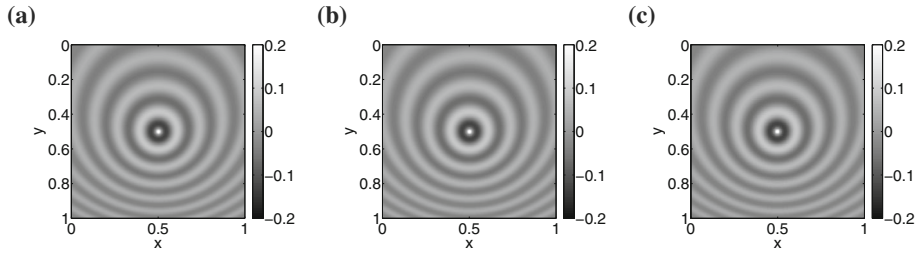

Fig. 12 Example 2: The wave field of **a** FDTD solution, **b** the one-term expansion w_0, and **c** the two-term expansion $w = w_0 + w_1$ with frequency $\omega = 8\pi$

v_0 is computed by the third-order Lax–Friedrichs WENO scheme with the fourth-order ($P = 4$) factorization around the source.

v_1 is computed by the third-order Lax–Friedrichs WENO scheme with the first-order ($P = 1$) factorization around the source.

The FDTD results are computed in the domain $[-0.1, 0.6]^3$ with mesh grid $141 \times 141 \times 141$ for $\omega = \pi$ and mesh grid $281 \times 281 \times 281$ for $\omega = 16\pi$.

Example 3 **a constant refractive index** The computational setup is the following.

- The refractive index $n(x, y, z) = 2$;
- The computational domain is $[0, 0.5] \times [0, 0.5] \times [0, 0.5]$;
- The mesh size is $50 \times 50 \times 50$ with the grid size $h = 0.01$;
- The angular frequency $\omega = \pi$ or 16π;
- The source point is $(0.25, 0.25, 0.25)$.

Figure 13 shows the errors of τ^2, $\frac{\partial}{\partial y}\tau^2$ and $\frac{\partial^2}{\partial y^2}\tau^2$ at $z = 0.25$. Figure 14 shows the error of v_0 along with the fields of Δv_0 and v_1 at $z = 0.25$.

Figure 15 shows the exact solution, the first term w_0, and the two-term expansion $w = w_0 + w_1$ at $z = 0.25$ for $\omega = \pi$. Figure 16 shows the results for $\omega = 16\pi$. More detailed comparisons are shown in Fig. 17 for $\omega = \pi$ and in Fig. 18 for $\omega = 16\pi$, respectively.

Example 4 **Constant gradient for** $\frac{1}{n}$ The computational setup is the following.

- The refractive index $n(x, y, z) = \dfrac{1}{0.5 - (y - 0.25)}$;
- The computational domain is $[0, 0.5] \times [0, 0.5] \times [0, 0.5]$;
- The mesh size is $50 \times 50 \times 50$;

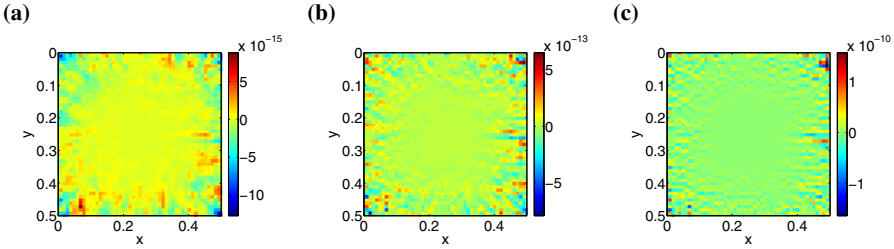

Fig. 13 Example 3: **a** The error of τ^2 at $z = 0.25$. **b** The error of $\frac{\partial}{\partial y}\tau^2$ at $z = 0.25$. **c** The error of $\frac{\partial^2}{\partial y^2}\tau^2$ at $z = 0.25$

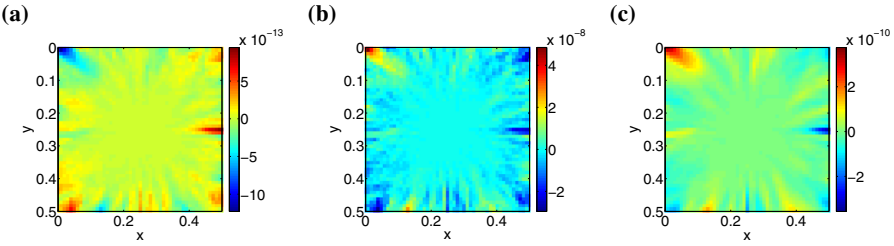

Fig. 14 Example 3: **a** The error of v_0 at $z = 0.25$. **b** The field of Δv_0 at $z = 0.25$. **c** The field of v_1 at $z = 0.25$.

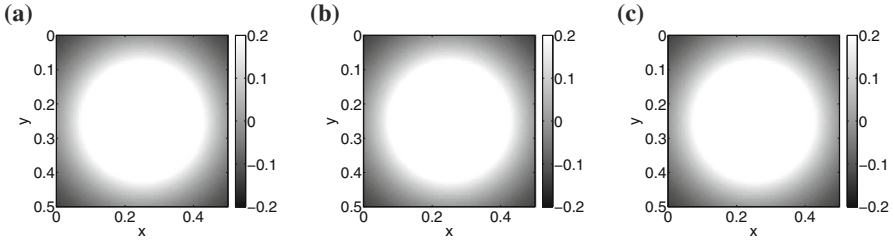

Fig. 15 Example 3: **a** The wave field of the exact solution at $z = 0.25$ with $\omega = \pi$. **b** The wave field of w_0 at $z = 0.25$ with $\omega = \pi$. **c** The wave field of $w = w_0 + w_1$ at $z = 0.25$ with $\omega = \pi$

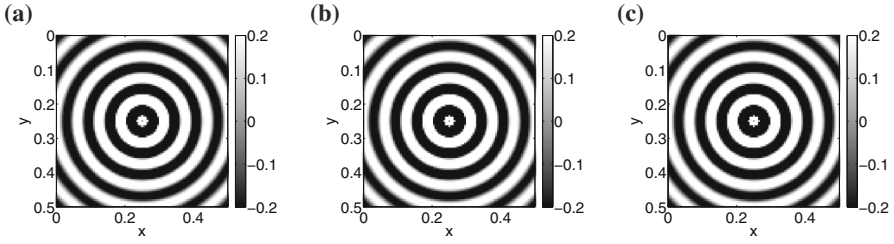

Fig. 16 Example 3: **a** The wave field of the exact solution at $z = 0.25$ with $\omega = 16\pi$. **b** The wave field of w_0 at $z = 0.25$ with $\omega = 16\pi$. **c** The wave field of $w = w_0 + w_1$ at $z = 0.25$ with $\omega = 16\pi$

- The angular frequency $\omega = \pi$ or 16π.
- The source point is $(0.25, 0.25, 0.25)$.

In this case, the exact solution for the phase τ can be computed.

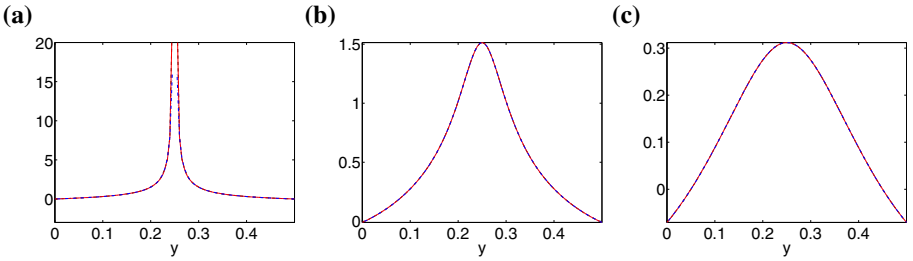

Fig. 17 Example 3: **a** The wave field at line $x = 0.25, z = 0.25$ with $\omega = \pi$. **b** The wave field at line $x = 0.2, z = 0.25$ with $\omega = \pi$. **c** The wave field at line $x = 0.1, z = 0.25$ with $\omega = \pi$. *Blue dash-dot line* exact solution; *black dashed line* one-term expansion w_0; *red solid line* two-term expansion $w = w_0 + w_1$ (Color figure online)

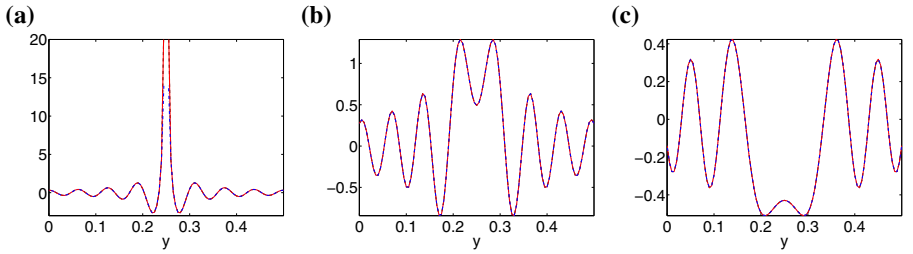

Fig. 18 Example 3: **a** The wave field at line $x = 0.25, z = 0.25$ with $\omega = 16\pi$. **b** The wave field at line $x = 0.2, z = 0.25$ with $\omega = 16\pi$. **c** The wave field at line $x = 0.1, z = 0.25$ with $\omega = 16\pi$. *Blue dash-dot line* exact solution; *black dashed line* one-term expansion w_0; *red solid line* two-term expansion $w = w_0 + w_1$ (Color figure online)

Table 2 Example 4: The l_1 and l_∞ errors of τ and its order of convergence

Mesh	$41 \times 41 \times 41$	$81 \times 81 \times 81$	$161 \times 161 \times 161$
l_∞	5.26×10^{-6}	1.42×10^{-7}	4.51×10^{-9}
Order		5.21	4.98
l_1	7.29×10^{-8}	1.60×10^{-9}	4.69×10^{-11}
Order		5.51	5.09

The phase τ is computed by the hybrid scheme with fifth-order multiplicative factorization and the fifth-order Lax–Friedrichs WENO scheme

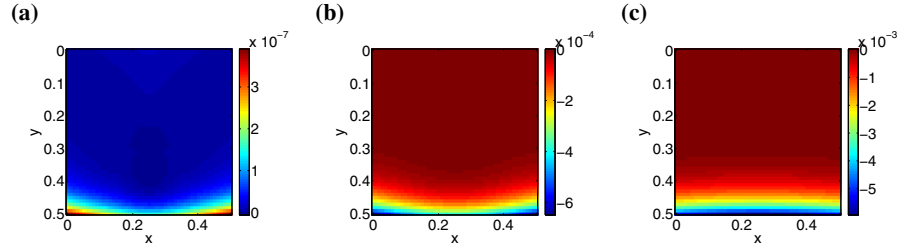

Fig. 19 Example 4: The error of **a** τ^2, **b** $\frac{\partial}{\partial y}\tau^2$, and **c** $\frac{\partial^2}{\partial y^2}\tau^2$ at $z = 0.25$

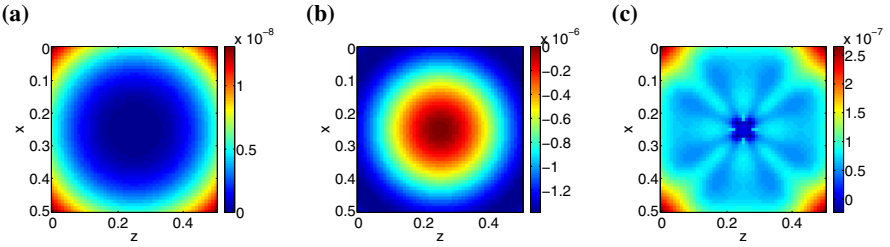

Fig. 20 Example 4: The error of **a** τ^2, **b** $\frac{\partial}{\partial y}\tau^2$, and **c** $\frac{\partial^2}{\partial y^2}\tau^2$ at $y = 0.25$.

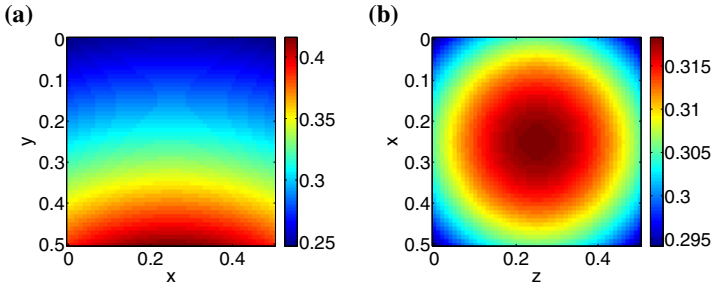

Fig. 21 Example 4: The field of v_0 at **a** $z = 0.25$ and **b** $y = 0.25$.

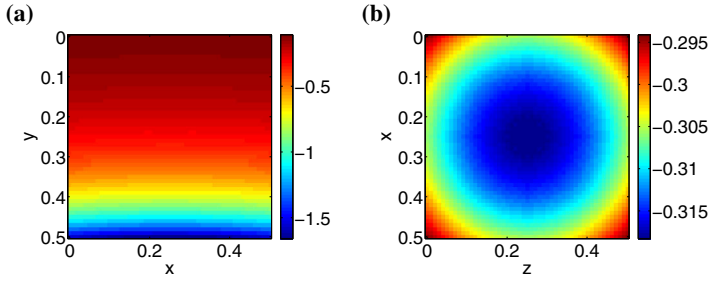

Fig. 22 Example 4: The field of Δv_0 at **a** $z = 0.25$ and **b** $y = 0.25$.

To validate that our method is of fifth-order accuracy for computing phase τ, we have computed the order of convergence of our method as shown in Table 2, which indicates fifth-order convergence in both l_1 and l_∞ norms.

Figure 19 shows the errors of τ^2, $\frac{\partial}{\partial y}\tau^2$ and $\frac{\partial^2}{\partial y^2}\tau^2$ at $z = 0.25$, while Fig. 20 show those errors at $y = 0.25$. Figure 21 shows the field of the first coefficient v_0 at $x = 0.25$ and $y = 0.25$, respectively. Figure 22 shows the field of Δv_0 at $z = 0.25$ and $y = 0.25$, respectively. Figure 23 shows the fields of the second coefficient v_1 at $z = 0.25$ and $y = 0.25$, respectively.

Figures 24 and 25 show the wave field with $\omega = \pi$ obtained by a direct method, the one-term expansion w_0, and the two-term expansion $w = w_0 + w_1$ at $y = 0.25$ and $z = 0.25$, respectively.

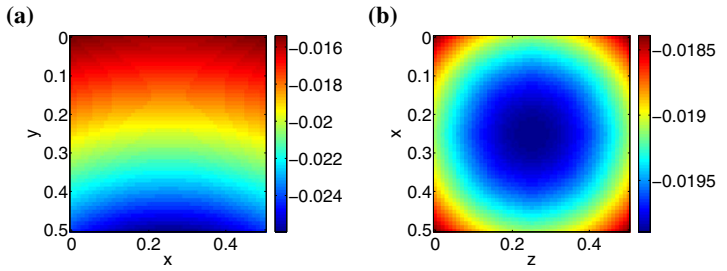

Fig. 23 Example 4: The field of v_1 at **a** $z = 0.25$ and **b** $y = 0.25$.

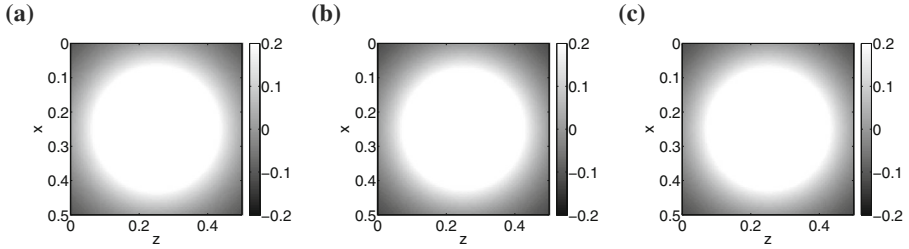

Fig. 24 Example 4: The wave field of **a** FDTD solution , **b** the one-term expansion w_0, and **c** the two-term expansion $w = w_0 + w_1$ at $y = 0.25$ with frequency $\omega = \pi$.

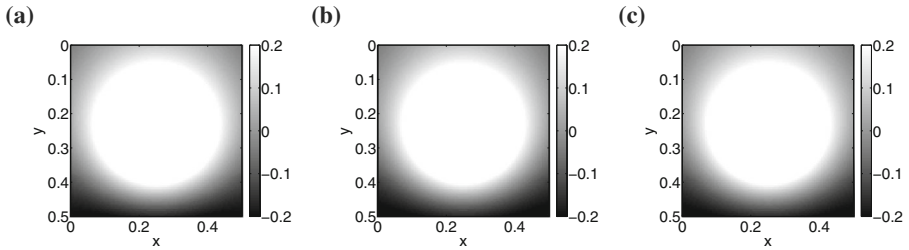

Fig. 25 Example 4: The wave field of **a** FDTD solution , **b** the one-term expansion w_0, and **c** the two-term expansion $w = w_0 + w_1$ at $z = 0.25$ with frequency $\omega = \pi$.

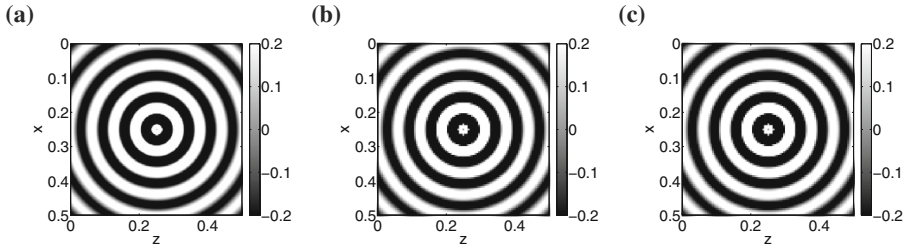

Fig. 26 Example 4: The wave field of **a** FDTD solution (25 points per wavelength), **b** the one-term expansion w_0, and **c** the two-term expansion $w = w_0 + w_1$ at $y = 0.25$ with frequency $\omega = 16\pi$.

Figure 26 shows the wave field at $y = 0.25$ with $\omega = 16\pi$ obtained by a direct method, the one-term expansion w_0, and the two-term expansion $w = w_0 + w_1$, where the direct method uses 25 points per wavelength; Fig. 27 shows similar results at $z = 0.25$.

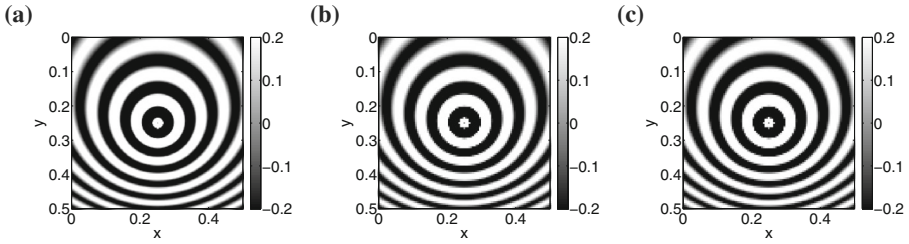

Fig. 27 Example 4: The wave field of **a** FDTD solution (25 points per wavelength), **b** the one-term expansion w_0, and **c** the two-term expansion $w = w_0 + w_1$ at $z = 0.25$ with frequency $\omega = 16\pi$.

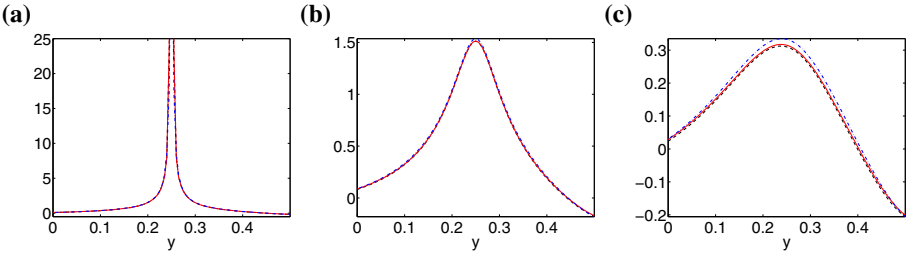

Fig. 28 Example 4: The wave field at line **a** $x = 0.25$, $z = 0.25$, **b** $x = 0.2$, $z = 0.25$, and **c** $x = 0.1$, $z = 0.25$ with frequency $\omega = \pi$. *Blue dash-dot line* FDTD solution; *black dashed line* one-term expansion w_0; *red solid line* two-term expansion $w = w_0 + w_1$ (Color figure online)

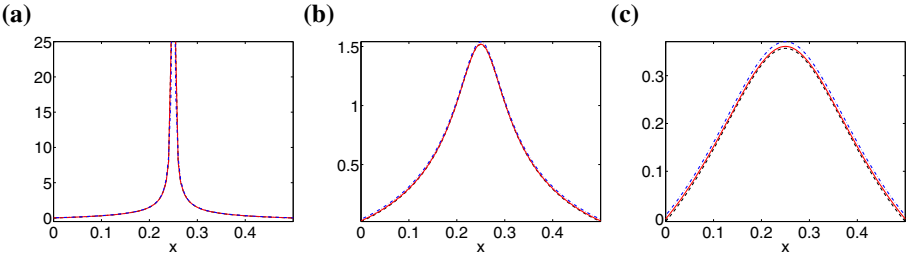

Fig. 29 Example 4: The wave field at line **a** $y = 0.25$, $z = 0.25$, **b** $y = 0.2$, $z = 0.25$, and **c** $y = 0.1$, $z = 0.25$ with frequency $\omega = \pi$. *Blue dash-dot line* FDTD solution; *black dashed line* one-term expansion w_0; *red solid line* two-term expansion $w = w_0 + w_1$ (Color figure online)

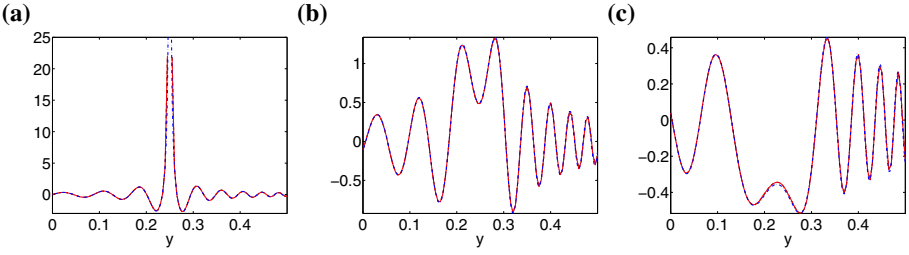

Fig. 30 Example 4: The wave field at line **a** $x = 0.25$, $z = 0.25$, **b** $x = 0.2$, $z = 0.25$, and **c** $x = 0.1$, $z = 0.25$ with frequency $\omega = 16\pi$. *Blue dash-dot line* FDTD solution; *black dashed line* one-term expansion w_0; *red solid line* two-term expansion $w = w_0 + w_1$ (Color figure online)

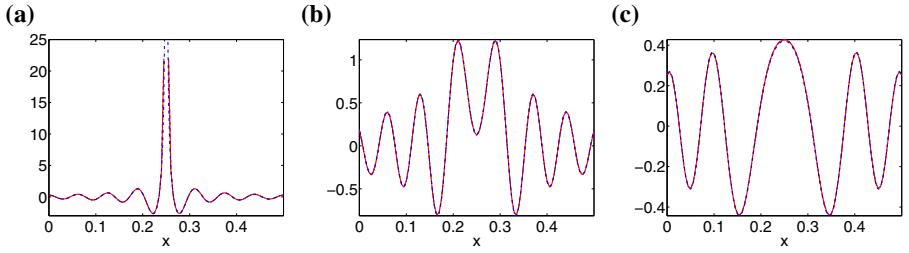

Fig. 31 Example 4: The wave field at line **a** $y = 0.25$, $z = 0.25$, **b** $y = 0.2$, $z = 0.25$, and $y = 0.1$, $z = 0.25$ with frequency $\omega = 16\pi$. *Blue dash-dot line* FDTD solution; *black dashed line* one-term expansion w_0; *red solid line* two-term expansion $w = w_0 + w_1$ (Color figure online)

Figure 28 shows the wave field with $\omega = \pi$ by a direct method, the one-term expansion, and the two-term expansion on three different lines, $x = 0.25$ and $z = 0.25$, $x = 0.2$ and $z = 0.25$, and $x = 0.1$ and $z = 0.25$, respectively. Figure 29 shows the results with $\omega = \pi$ for another set of three different lines.

Similar results are shown in Figs. 30 and 31 for $\omega = 16\pi$.

7 Conclusion

Starting from Babich's expansion, we develop high-order Eulerian asymptotics for Helmholtz equations in inhomogeneous media. Both the eikonal and transport equations are solved by high-order Lax–Friedrichs weighted non-oscillatory schemes. We also prove that fifth-order Lax–Friedrichs WENO schemes for eikonal equations are convergent when the eikonal is smooth. Numerical examples demonstrate effectiveness and accuracy of the new methods. Moreover, since Babich's ansatz is closely related to Hadamard's method of forming the fundamental solution of the Cauchy problem for the time-dependent wave equation [3], we can apply our high-order Eulerian asymptotic methods for constructing the fundamental solution of the time-dependent wave equation as well, which is an ongoing project.

Acknowledgments Qian is supported by NSF Grants DMS-1222368 and DMS-1522249. Yuan is partially supported by the National Natural Science Foundation of China (Project No. 11201508).

References

1. Abramowitz, M., Stegun, I.A.: Handbook of Mathematical Functions. Dover Publications, Inc., New York (1965)
2. Avila, G.S., Keller, J.B.: The high-frequency asymptotic field of a point source in an inhomogeneous medium. Commun. Pure Appl. Math. **16**, 363–381 (1963)
3. Babich, V.M.: The short wave asymptotic form of the solution for the problem of a point source in an inhomogeneous medium. USSR Comput. Math. Math. Phys. **5**(5), 247–251 (1965)
4. Benamou, J.D.: An introduction to Eulerian geometrical optics (1992–2002). J. Sci. Comput. **19**, 63–93 (2003)
5. Berman, A., Plemmons, R.J.: Nonnegative Matrices in the Mathematical Sciences. Academic Press, New York (1979)
6. Coddington, E., Levinson, N.: Theory of Ordinary Differential Equations. McGraw-Hill Book Company, Inc., New York, Toronto, London (1955)
7. Fomel, S., Luo, S., Zhao, H.-K.: Fast sweeping method for the factored eikonal equation. J. Comput. Phys. **228**(17), 6440–6455 (2009)

8. Jiang, G.S., Peng, D.: Weighted ENO schemes for Hamilton–Jacobi equations. SIAM J. Sci. Comput. **21**, 2126–2143 (2000)
9. Jiang, G.S., Shu, C.W.: Efficient implementation of weighted ENO schemes. J. Comput. Phys. **126**, 202–228 (1996)
10. Kao, C.Y., Osher, S.J., Qian, J.: Lax–Friedrichs sweeping schemes for static Hamilton–Jacobi equations. J. Comput. Phys. **196**, 367–391 (2004)
11. LeVeque, R.: Finite difference methods for ordinary and partial differential equations: steady-state and time-dependent problems. Society for Industrial and Applied Mathematics (SIAM), Philadelphia, Pennsylvania (2007)
12. Luo, S., Qian, J.: Factored singularities and high-order Lax–Friedrichs sweeping schemes for point-source traveltimes and amplitudes. J. Comput. Phys. **230**, 4742–4755 (2011)
13. Luo, S., Qian, J.: Fast sweeping methods for factored anisotropic eikonal equations: multiplicative and additive factors. J. Sci. Comput. **52**, 360–382 (2012)
14. Luo, S., Qian, J., Burridge, R.: Fast Huygens sweeping methods for Helmholtz equations in inhomogeneous media in the high frequency regime. J. Comput. Phys. **270**, 378–401 (2014)
15. Luo, S., Qian, J., Burridge, R.: High-order factorization based high-order hybrid fast sweeping methods for point-source eikonal equations. SIAM J. Numer. Anal. **52**, 23–44 (2014)
16. Luo, S., Qian, J., Zhao, H.-K.: Higher-order schemes for 3-D traveltimes and amplitudes. Geophysics **77**, T47–T56 (2012)
17. Milnor, J.: Morse Theory. Annals of Mathematic No. 51. Princeton University Press, Princeton, New Jersey (1973)
18. Ortega, J.: Matrix Theory, a Second Course. Plenum Press, New York (1987)
19. Pica, A.: Fast and accurate finite-difference solutions of the 3D eikonal equation parametrized in celerity. In: 67th Annal International Meeting Society of Exploration Geophysicists, pp. 1774–1777 (1997)
20. Qian, J., Symes, W.W.: An adaptive finite difference method for traveltime and amplitude. Geophysics **67**, 167–176 (2002)
21. Serna, S., Qian, J.: A stopping criterion for higher-order sweeping schemes for static Hamilton–Jacobi equations. J. Comput. Math. **28**, 552–568 (2010)
22. Strang, G.: Accurate partial difference methods II. Non-linear problems. Numer. Math. **6**, 37–46 (1964)
23. Symes, W.W., Qian, J.: A slowness matching Eulerian method for multivalued solutions of eikonal equations. J. Sci. Comput. **19**, 501–526 (2003)
24. Vidale, J.E., Houston, H.: Rapid calculation of seismic amplitudes. Geophysics **55**, 1504–1507 (1990)
25. Xiong, T., Zhang, M., Zhang, Y.T., Shu, C.-W.: Fast sweeping fifth order weno scheme for static Hamilton–Jacobi equations with accurate boundary treatment. J. Sci. Comput. **45**, 514–536 (2010)
26. Zhang, L., Rector, J.W., Hoversten, G.M.: Eikonal solver in the celerity domain. Geophys. J. Int. **162**, 1–8 (2005)
27. Zhang, Y.T., Zhao, H.K., Qian, J.: High order fast sweeping methods for static Hamilton–Jacobi equations. J. Sci. Comput. **29**, 25–56 (2006)